Technical report

Analysis of sub-mesoscale structures in the north-western Mediterranean by comparing in-situ and satellite data

Fernando Becker

Introduction

The Mediterranean Sea is a semi-enclosed basin characterized as an evaporation-dominated system (evaporation > precipitation), functioning as a water mass transformation site. Surface waters enter from the Atlantic Ocean through the Strait of Gibraltar and circulate counterclockwise due to the Coriolis effect. These modified waters are ultimately exported westward through the deep layers of the Strait of Gibraltar as a denser water mass. This outflow, detectable between 1000-1200 m depth, forms a distinct water mass that can be traced throughout the North Atlantic Ocean (Le Vourch, 1992; Millot & Taupier-Letage, 2005).

In the Northwestern Mediterranean (NWM), the large-scale circulation is dominated by the Northern Current, which forms in the Ligurian Sea through the convergence of the Western Corsica Current (WCC) and Eastern Corsica Current (ECC) (Palomera et al., 2007). The NWM is further influenced by mesoscale anticyclonic eddies generated through barotropic and baroclinic instabilities of the Algerian Current along the southern basin margin. These eddies play a crucial role in redistributing water masses toward the central basin (Fig. 1; Millot, 1999).

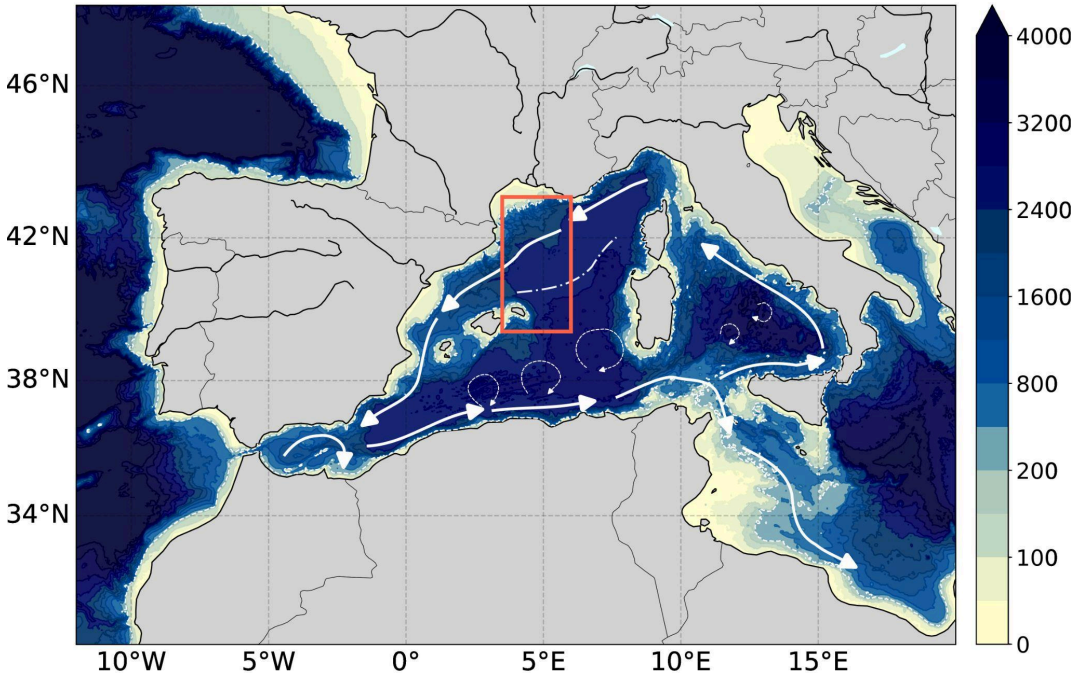

Fig. 1: General circulation of the Western Mediterranean Sea (adapted from Millot & Taupier-Letage 2005). Solid white arrows indicate mean currents, dashed lines denote transient eddies, and a dash-dotted line marks the North Balearic Front region. The red rectangle outlines the study area of the 2023 BioSWOT-Med cruise.

The North Balearic Front results as the northern boundary of the Atlantic Water (AW) reservoir in the Algerian Basin, separating the newer, less dense Atlantic waters (to the south) from the older, denser Mediterranean waters (modified Atlantic Water, mAW) to the north (Millot, 1987). Oceanic fronts are characterized by complex dynamics associated with mesoscale and submesoscale structures. These structures—particularly submesoscale eddies—exhibit vertical velocities up to an order of magnitude greater than those at mesoscale (McWilliams et al., 2016; Zatsepin et al., 2019), with spatial scales of ~10 km and

time scales ranging from hours to several days (Thomas et al., 2008; McWilliams et al., 2016; Zatsepin et al., 2019). Their relevance lies in their critical role in ocean-atmosphere interaction (Mahadevan, 2016) and the transport of biogeochemical properties, such as nutrients and heat (Su et al., 2018; Siegelman et al., 2020; Chen et al., 2022; Strobach et al., 2022; Conejero et al., 2024).
Despite their importance, submesoscale eddies have been far less studied compared to larger-scale structures. Previous research has characterized them using optical satellite imagery (Zhang et al., 2019; Becker et al., 2023) and high-resolution numerical modeling (Capet et al., 2008; Cao et al., 2021; Gula et al., 2016). Recent advances from the SWOT satellite have enabled further progress in studying these features through high space and time resolution novel altimetry data (Zhang et al., 2024; Doglioli et al., 2024).

This study presents the results obtained during a two-month research internship funded by the POGO-SCOR 2024 Fellowship at the Mediterranean Institute of Oceanography (MIO). The work focused on analyzing data from the BioSWOT-Med 2023 cruise (from 21 April to 15 May 2023), a multidisciplinary oceanographic campaign designed for SWOT altimeter calibration and validation.

Data and Methodology

The study has integrated multi-platform datasets to ensure robust comparisons. VIIRS[1] level 2 imagery and Sentinel-3[2] data (obtained from the Copernicus Open Access Hub) provided daily chlorophyll-a and sea surface temperature (SST) fields at 750 and 300 m spatial resolution, respectively. SWOT[3] altimetry v2.0 data offered high-resolution absolute dynamic topography (ADT) at 2 km resolution with daily temporal coverage. For broader-scale context, DUACS[4] delayed-time altimetry ADT products (Copernicus Marine Service) were used, featuring a 25 km spatial and daily temporal resolution.

The submesoscale eddy detection algorithm developed by Becker et al. (2023) was adapted to the Mediterranean region. This algorithm uses chlorophyll-a and SST values from VIIRS and Sentinel-3 to identify coherent submesoscale eddies.
To assess the accuracy of altimetry-derived currents, geostrophic velocities from SWOT and DUACS products were compared with shipboard ADCP measurements (hull-mounted, RDI Ocean Surveyor - os38 / Frequency (kHz) 38 / Vertical resolution (m) 12 / Depth range (m) 42-990 / Number of bins 80) collected synchronously during the BioSWOT-Med cruise.

Results and Discussion

Algorithm

The algorithm developed by Becker et al. (2023) was adapted and applied to available VIIRS imagery from the Northwest Mediterranean (NWM) region for the period 15 April to 20 May 2023 to identify submesoscale eddies. All the analyses described below were performed for

[1]https://search.earthdata.nasa.gov/search?q=10.5067/NOAA-21/VIIRS/L2/OC/2022
[2]https://search.earthdata.nasa.gov/search?fi=OLCI&gdf=NetCDF
[3]https://tds-odatis.aviso.altimetry.fr/thredds/catalog/dataset-l3-swot-karin-nadir-validated/l3_lr_ssh/v2_0/Expert/catalog.html
[4]https://data.marine.copernicus.eu/product/SEALEVEL_EUR_PHY_L4_MY_008_068/download?dataset=cmems_obs-sl_eur_phy-ssh_my_allsat-l4-duacs-0.0625deg_P1D_202411

all available images, but only two dates will be shown as examples, the rest of the material is available in a supplementary material. A special focus was made on the date May 4, 2023, when multiple drifters were deployed during the BioSWOT-Med cruise on a submesoscale anticyclonic eddy located near 40.5°N, 5°E (Fig. 2, left).

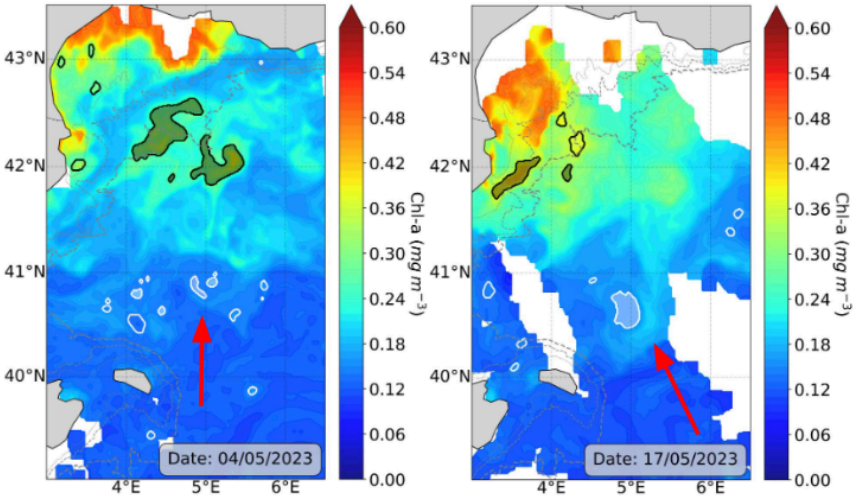

Fig. 2: VIIRS Level 2 chlorophyll-a concentration from 4 and 17 May, left and right respectively. Solid black (white) contours denote algorithm-detected as potentially cyclonic (anticyclonic) eddies using chlorophyll data alone, while gray (white) filled areas represent potential eddies detected by both chlorophyll and SST data. The red arrows mark the anticyclonic eddy where the drifters were deployed during the BioSWOT-Med cruise. Dashed contours indicate the 200, 1000, and 2000 m isobaths.

The analysis revealed that the algorithm did not correctly detect this eddy. A potential reason for this detection failure may stem from the algorithm's reliance on sea surface temperature (SST) imagery, which is often unreliable over the Mediterranean region due to the Mistral wind effects. These strong northerly winds can significantly modify sea surface temperature patterns, masking the thermal signal characteristic of anticyclonic eddy dynamics. Another possible reason is the spiral-shaped chlorophyll signature of the eddy observed on 4 May, which may have prevented detection since the algorithm is designed to identify closed-contour features. Moreover, later images from May 17 show the same eddy with a smoother chlorophyll signal that lacks the spiral pattern, allowing the correct detection of the algorithm (Fig. 2, right). It is important to note that by May 17th the BioSWOT-Med campaign had concluded and no in situ measurements were available for validation. The algorithm presented a similar limitation with the spiral topographic eddies generated at the mouth of the San Jose Gulf, on the Argentine continental shelf.

VIIRS/Sentinel-3 and SWOT

Several small-scale features visible in VIIRS and Sentinel-3 chlorophyll images were analyzed from ADT, geostrophic velocity and vorticity provided by SWOT. To enable a more detailed analysis in selected regions, data were extracted along predefined transects (Fig. 3-7).

In the SWOT image of May 4th, two anticyclonic eddies are observed near 40.5°N - 5°E and 42°N - 4.5°E. A cyclonic eddy is also detected in the vicinity of 42°N - 5°E (Fig.3 a). In transect 1 (Fig. 4, to the north), a sign change in vorticity is shown along with a sign change

in ADT. Both VIIRS and Sentinel-3 chlorophyll-a products show a local maximum in the same region, while the local maximum vorticity signal and local minimum ADT signal are observed slightly shifted to the east, approximately 10 km (Fig. 4). Over transect 2 (Fig. 5, to the south) a smooth local maximum of ADT is observed. The sign of the vorticity is mostly negative and consistent with the sign of the ADT, although with a significantly noisier signal than that shown at transect 1. Both chlorophyll-a products also show a noisy signal of small spatial scale, with no clear shape or pattern. This may have been another factor preventing clear detection of eddy, adding another possible cause to the previous section.

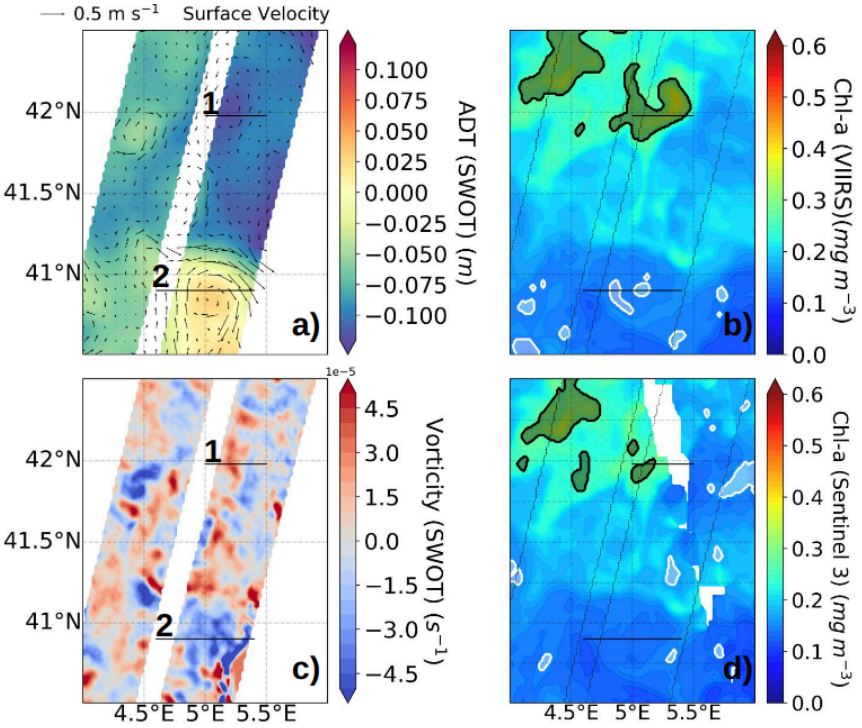

Fig.3: Altimetry and chlorophyll-a images for May 4. (a) Geostrophic velocities (in vectors) and ADT data from SWOT; (b) VIIRS L2 chlorophyll-a product with regions detected as potential cyclonic (black) and anticyclonic eddies (white); (c) vorticity from SWOT; (d) Sentinel-3 L2 chlorophyll-a with closed contours detected as potential cyclonic (black) and anticyclonic eddies (white). Solid black lines show transects from which values were extracted.

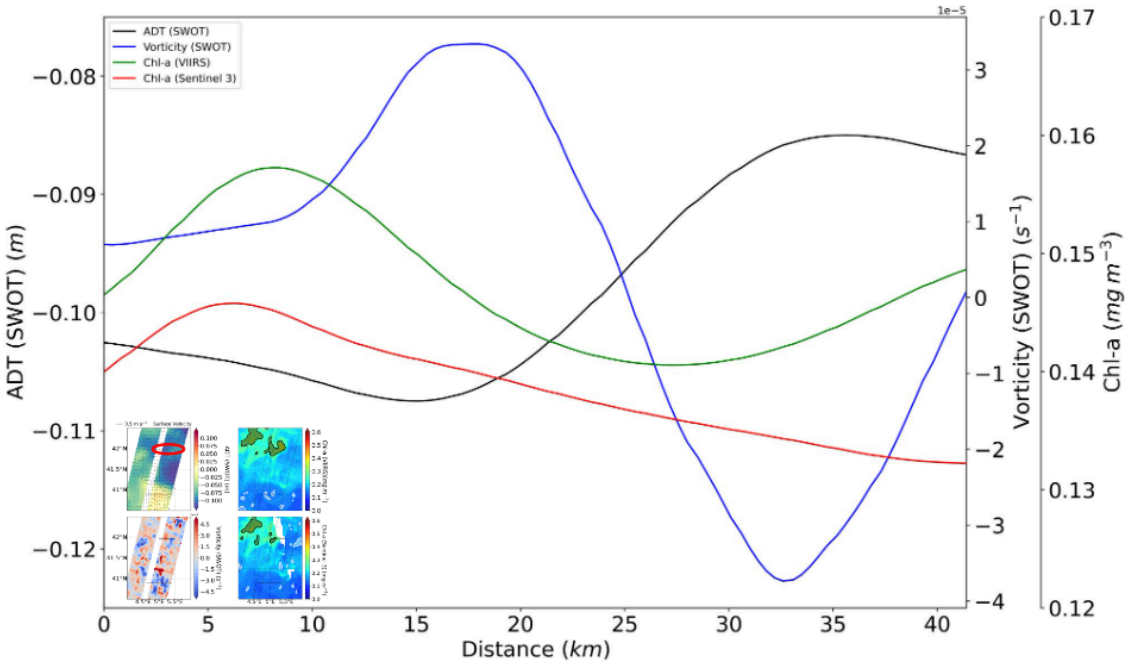

Fig.4: Transect 1 shown in Fig. 3. The ADT and vorticity from SWOT are shown in black and blue, respectively. The chlorophyll-a concentration from VIIRS and Sentinel-3 in green and red, respectively. A slight shift is observed between chlorophyll products and the signal shown by SWOT.

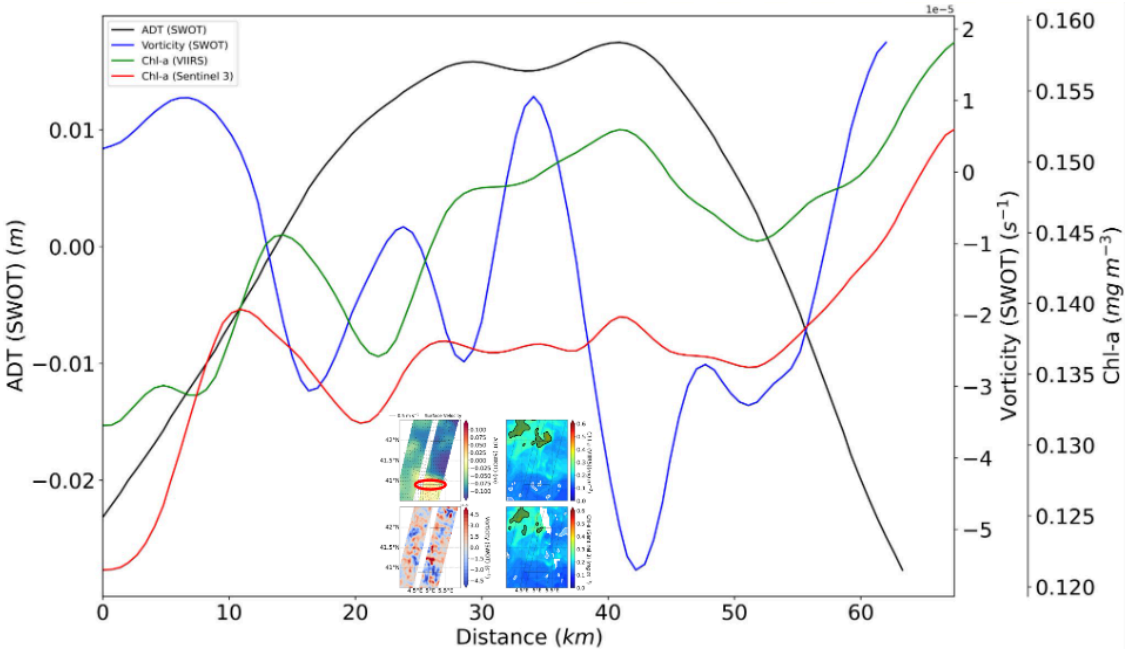

Fig.5: Transect 2 shown in Fig. 3. The ADT and vorticity from SWOT are shown in black and blue, respectively. chlorophyll-a concentrations from VIIRS and Sentinel-3 in green and red, respectively.

The SWOT image of May 17th shows the anticyclonic eddy at approximately 40.5°N - 5°E (Fig. 6). The anticyclonic signal is observed over all variables, showing a local maximum in the ADT and local minima in the vorticity and chlorophyll-a values. As in the previous date,

SWOT data are displaced to the east, approximately 10 km. A sharp change in the sign of vorticity is also observed to the west of the transect, which is reflected in high velocity values. This point will be better addressed in the next section.

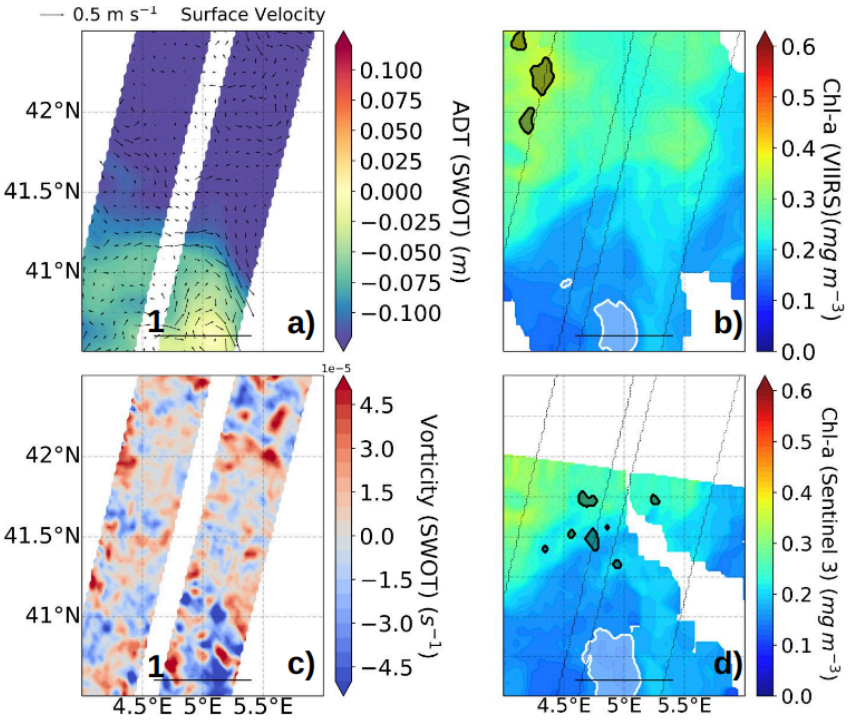

Fig.6: Altimetry and chlorophyll-a images for May 17. (a) ADT and geostrophic velocity products (in vectors) from SWOT; (b) VIIRS L2 chlorophyll-a product with regions detected as potential cyclonic eddies (black) and anticyclonic (white); (c) vorticity from SWOT; (d) Sentinel-3 L2 chlorophyll-a product with regions detected as potential cyclonic eddies (black) and anticyclonic (white). Solid black lines show transects from which values were extracted.

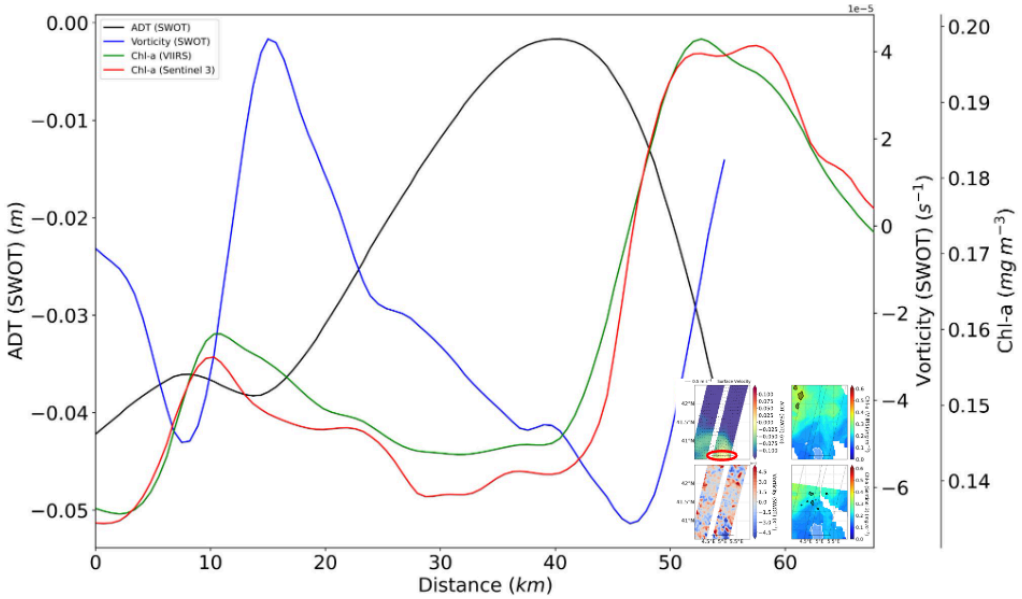

Fig.7: Transect 1 shown in Fig. 6. The ADT and vorticity from SWOT are shown in black and blue, respectively. The chlorophyll-a signal from VIIRS and Sentinel-3 products in green and

red, respectively. A slight offset is observed between the chlorophyll signals of both products and the signal shown by SWOT.

SWOT vs DUACS

DUACS images were downloaded for the same date range, and a comparison was made with the ADT product provided by SWOT. The ADT differences between the two products and the differences between velocity magnitudes were calculated. The SWOT products described the ADT and velocity fields in better detail due to their higher spatial resolution. On transect 1, a maximum of velocity magnitude differences are highlighted (Fig. 8 f), which corresponds to a chlorophyll-a filament detaching in a southerly direction from a cyclonic gyre located at approximately 42°N - 5°E. The values extracted along the transect reveal the higher spatial resolution of SWOT showing an evident change of sign in vorticity and ADT, which generate an intense jet. These features are not detected in the ADT and velocity values provided by DUACS due to their lower spatial resolution.

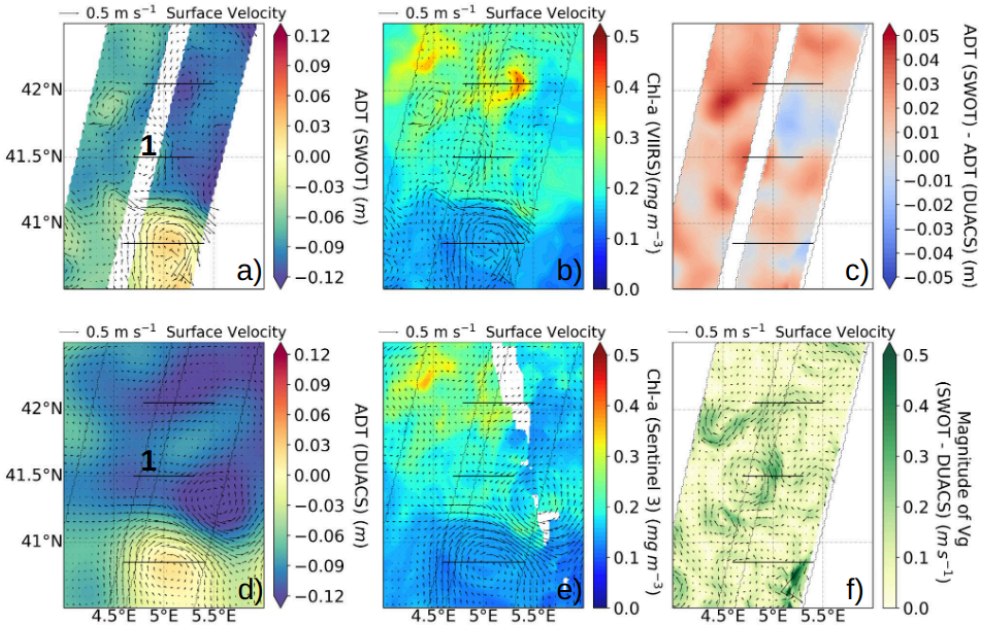

Fig.8: Altimetry and chlorophyll-a images of May 4. (a) ADT and SWOT geostrophic velocity; (b) VIIRS chlorophyll-a product; (c) difference between SWOT - DUACS ADT products; (d) ADT and DUACS geostrophic velocity; (e) Sentinel-3 chlorophyll-a product; (f) difference between SWOT - DUACS geostrophic velocity products. On transect 1 a local maximum discrepancy between both geostrophic velocities is observed, coinciding with an observable filament in both chlorophyll-a products with north-south direction.

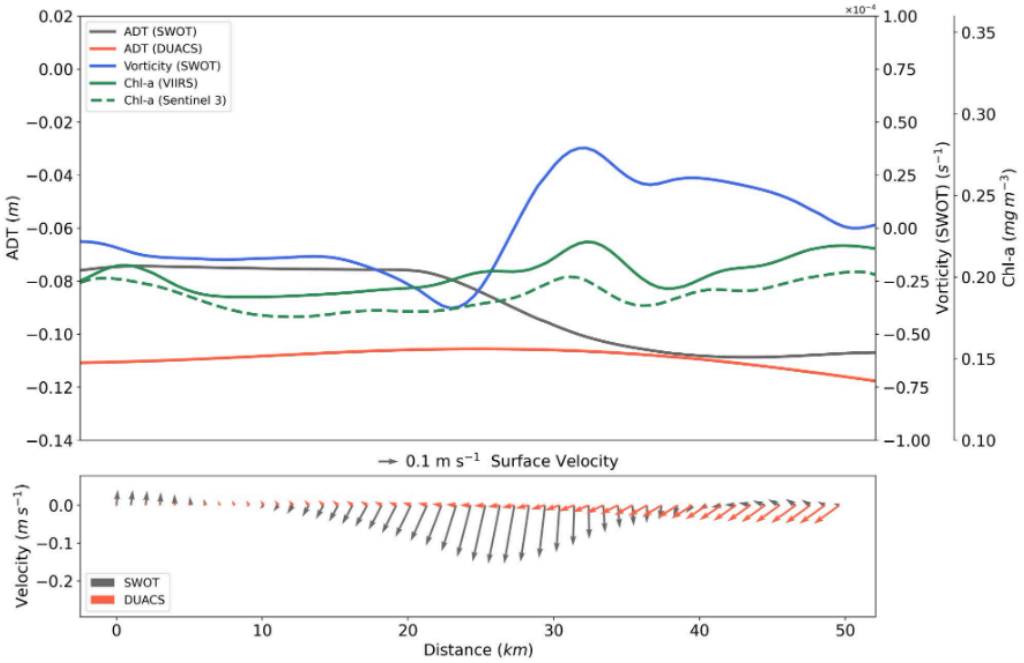

Fig.9: Values extracted from transect 1 shown in Fig. 8. The upper panel shows SWOT ADT (black), DUACS ADT (red), vorticity (blue), VIIRS chlorophyll-a (solid green) and Sentinel-3 (dashed green). The lower panel shows SWOT (black) and DUACS (red) geostrophic velocities. A southward jet in velocity is seen in the SWOT product not identifiable in DUACS.

For the images corresponding to May 17, a local maximum in the geostrophic velocity magnitude differences near 40.5°N - 4.7°E is observed (Fig. 10 f). The SWOT velocity values over the transect show a deflection that corresponds to a variation in ADT and a change of sign in vorticity, a feature that is not observed in the DUACS products (Fig. 11). The characteristics of the large-scale velocity profile are well described by both products. The chlorophyll-a values, as in the previous point, share the same behavior and very similar values.

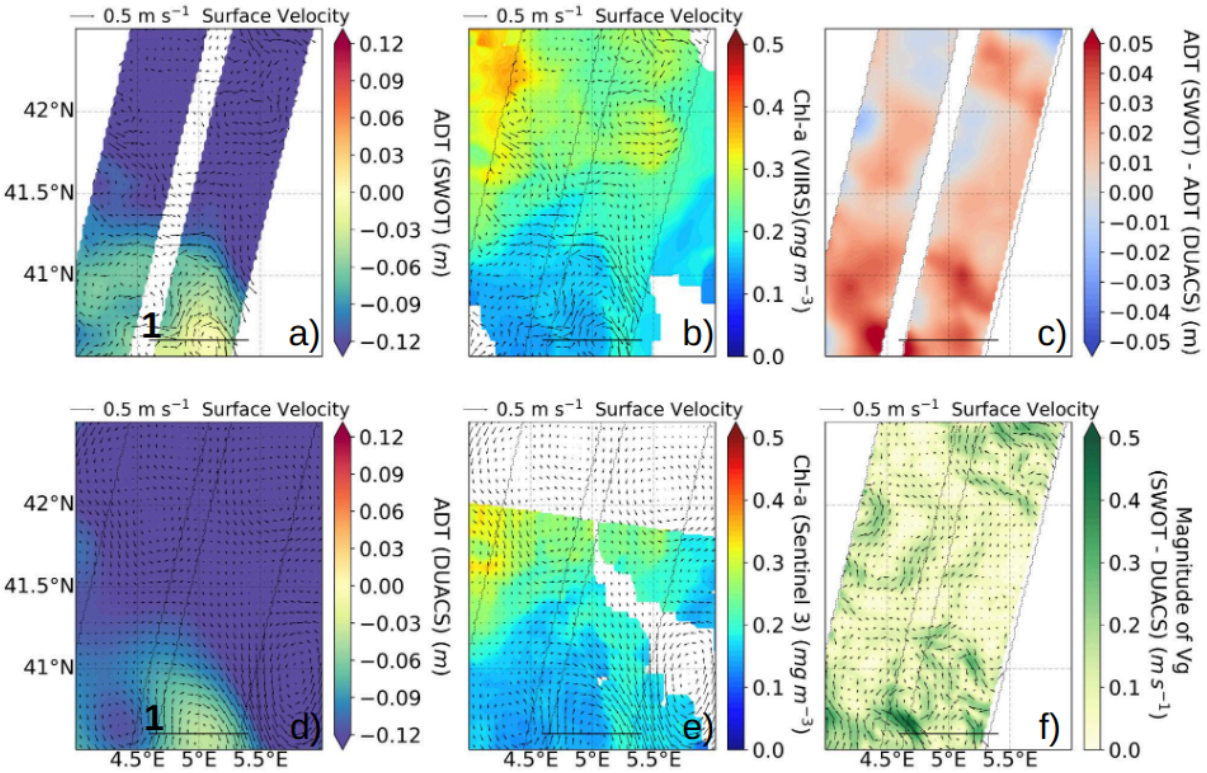

Fig.10: Altimetry and chlorophyll-a images of May 17. (a) SWOT ADT and geostrophic velocity; (b) VIIRS chlorophyll-a product; (c) difference between SWOT - DUACS ADT products; (d) DUACS ADT and geostrophic velocity; (e) Sentinel-3 chlorophyll-a product; (f) difference between SWOT - DUACS geostrophic velocity products. The SWOT velocity field shows a velocity deflection over transect 1 not observable in the DUACS velocity field.

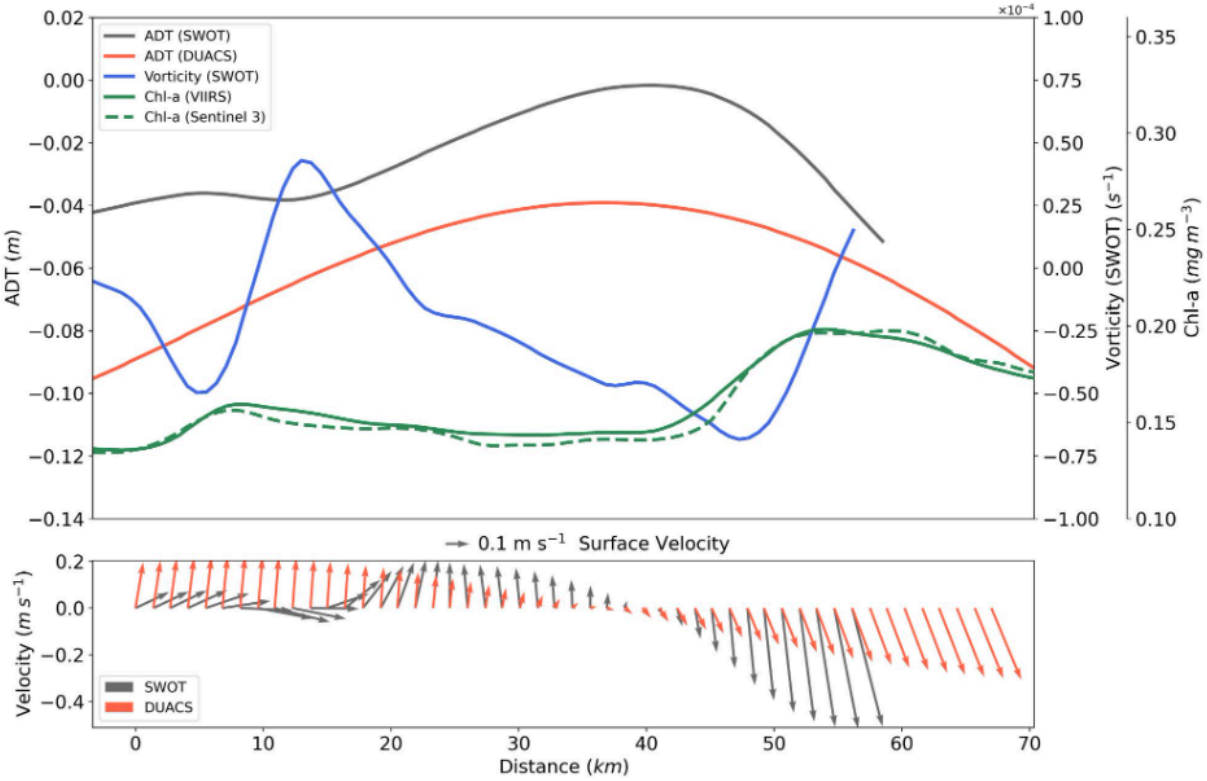

Fig.11: Values extracted from transect 1 shown in Fig. 10. The upper panel shows SWOT ADT (black), DUACS ADT (red), vorticity (blue), VIIRS chlorophyll-a (solid green) and Sentinel-3 (dashed green). The lower panel shows geostrophic velocities from SWOT (black) and DUACS (red). The SWOT velocity shows a velocity deflection over transect 1 not observable in the DUACS velocity.

Geostrophic velocity comparison of altimeter vs. vessel's ADCP

Lastly, a comparison was made between the geostrophic velocities of both altimeters and those provided by the vessel's ADCP during the BioSWOT-Med cruise. For this purpose, three transects were considered where the ship maintained a trajectory with no significant changes in direction.

Between April 30 and May 1 the vessel sailed over 5°E from 41.4°N to 39.8°N (Fig. 12). Along this trajectory the vessel crossed the Balearic front, a zonal front located at approximately 40.8°N that divides two water masses. This front is a natural barrier, leaving waters with higher chlorophyll-a concentration to the north and lower chlorophyll-a concentration to the south. This signal was observed with both satellite chlorophyll-a products (Fig. 13, top panel). Vertical velocities associated with submesoscale structures such as this front could generate the nutrient input necessary for their support. The ADT values of both altimeters showed similar behaviors with positive values to the south and negative values to the north of the front. This change corresponds to a local minimum of vorticity. Over the front region, the ship's ADCP observed intense zonal velocities, which were well represented by SWOT although slightly overestimated (Fig. 13, lower panel). The velocities given by DUACS, on the other hand, show near-zero values without detecting this feature in the velocity field.

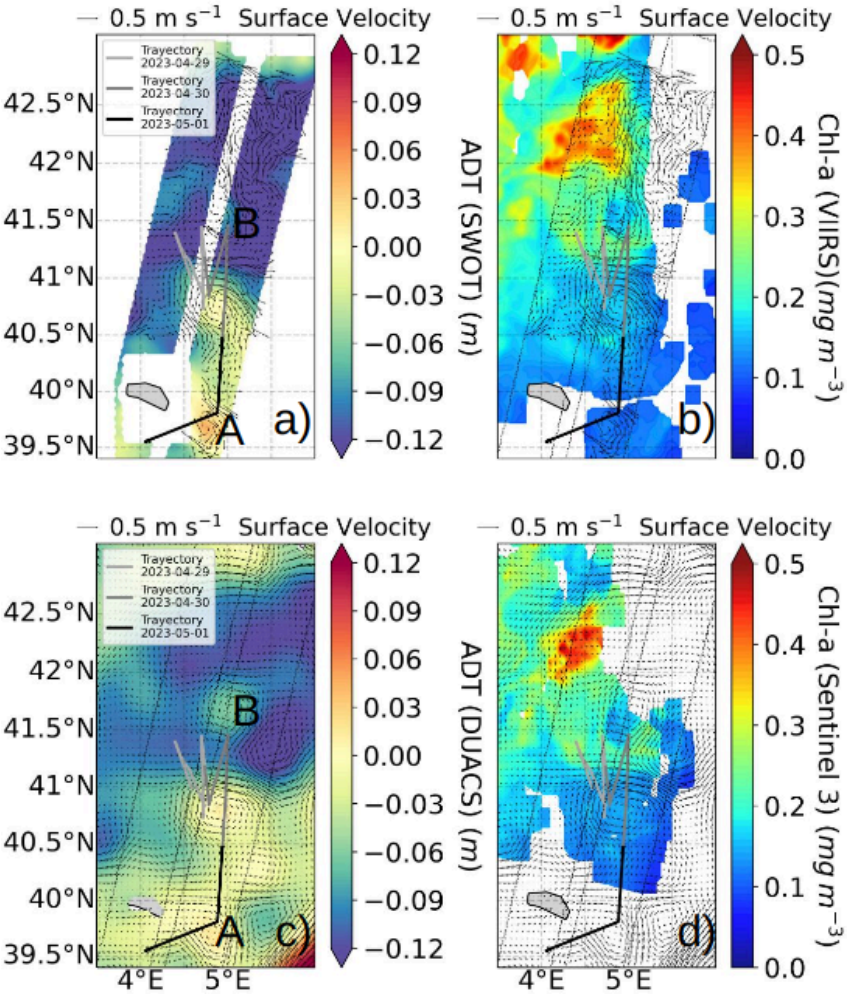

Fig. 12: Altimetry and chlorophyll-a images of April 30. (a) SWOT ADT and geostrophic velocity; (b) VIIRS chlorophyll-a product; (c) DUACS ADT and geostrophic velocity; (d) Sentinel-3 chlorophyll-a product. The vessel's trajectory between April 29 and May 1 is shown in shades of gray and black. Transect “A-B” is shown in Fig. 13.

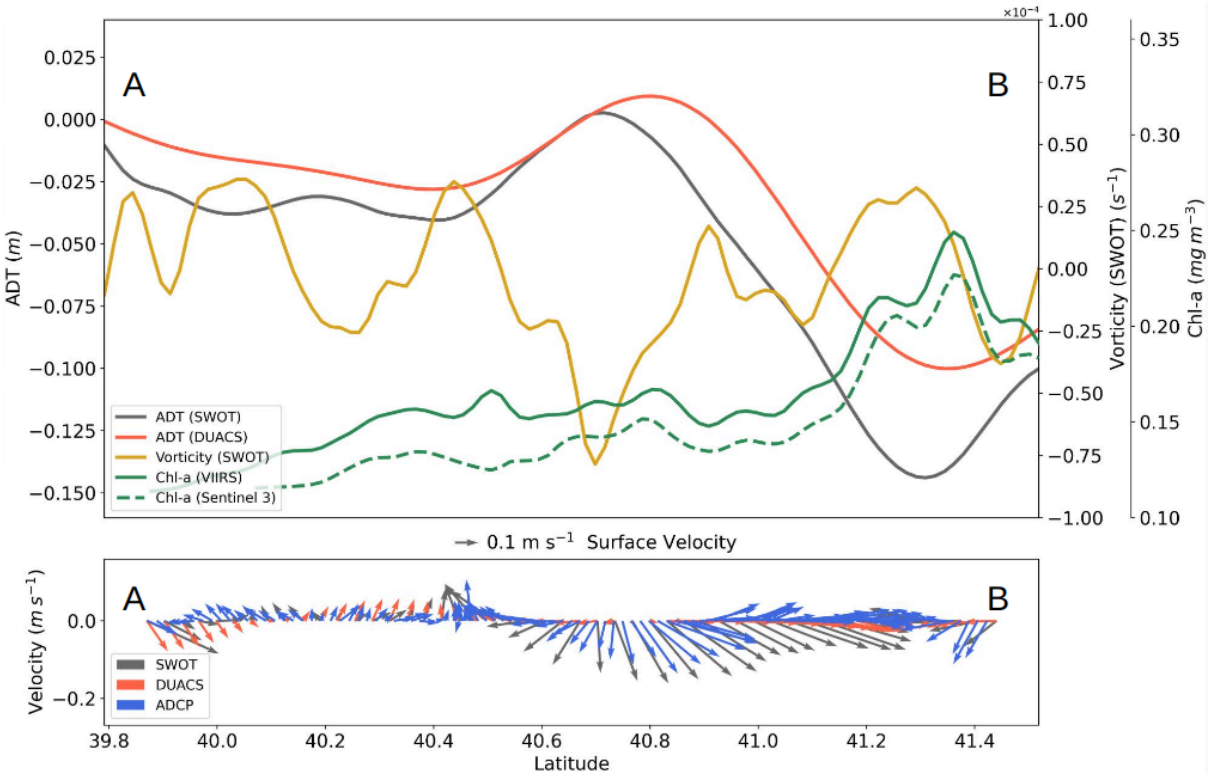

Fig.13: Values extracted from transect “A-B” shown in Fig. 12. The upper panel shows SWOT ADT (black), DUACS ADT (red), vorticity (yellow), VIIRS chlorophyll-a (solid green) and Sentinel-3 (dashed green). The lower panel shows SWOT geostrophic velocities (black), DUACS (red) and ship ADCP (blue). A jet detected by SWOT and the ship's ADCP is observed in the vicinity of the Balearic front.

During May 3, the vessel performed a south-north transect from 39.8°N to 40.8°N (transect “A-B” Fig. 14). Along this transect, both altimeters described similar behaviors, as well as the chlorophyll-a products. Regarding the velocities, the products given by the altimeters disagreed in both magnitude and direction with those measured by the ADCP between 39.8 and 40.2°N. Further to the north, there is a good agreement between both three products in terms of velocity direction, although DUACS presents an underestimation of the magnitude between 40.2 and 40.5°N.

During May 5, the vessel performed a southwest-northeast transect (transect “C-D” Fig. 14). The values of both altimeters, as well as the chlorophyll-a products, described similar behaviors. The velocities measured by the ADCP were well represented by the altimeters in terms of their direction, although both underestimated their magnitude up to about 41.1°N.

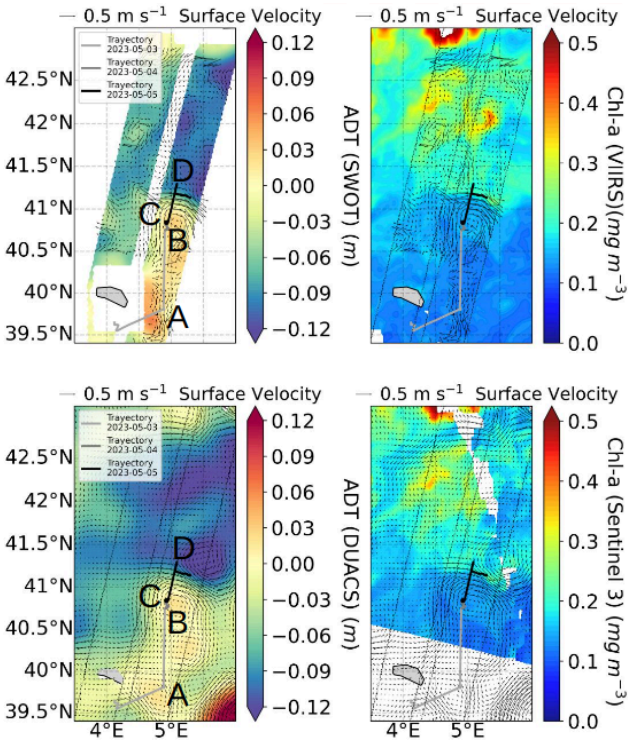

Fig. 14: Altimetry and chlorophyll-a images of May 4. (a) SWOT ADT and geostrophic velocity; (b) VIIRS chlorophyll-a product; (c) DUACS ADT and geostrophic velocity; (d) Sentinel-3 chlorophyll-a product. The ship's trajectory between April 29 and May 1 is shown in shades of gray and black. Transect “A-B” and “C-D” are shown in Fig. 15 and 16, respectively.

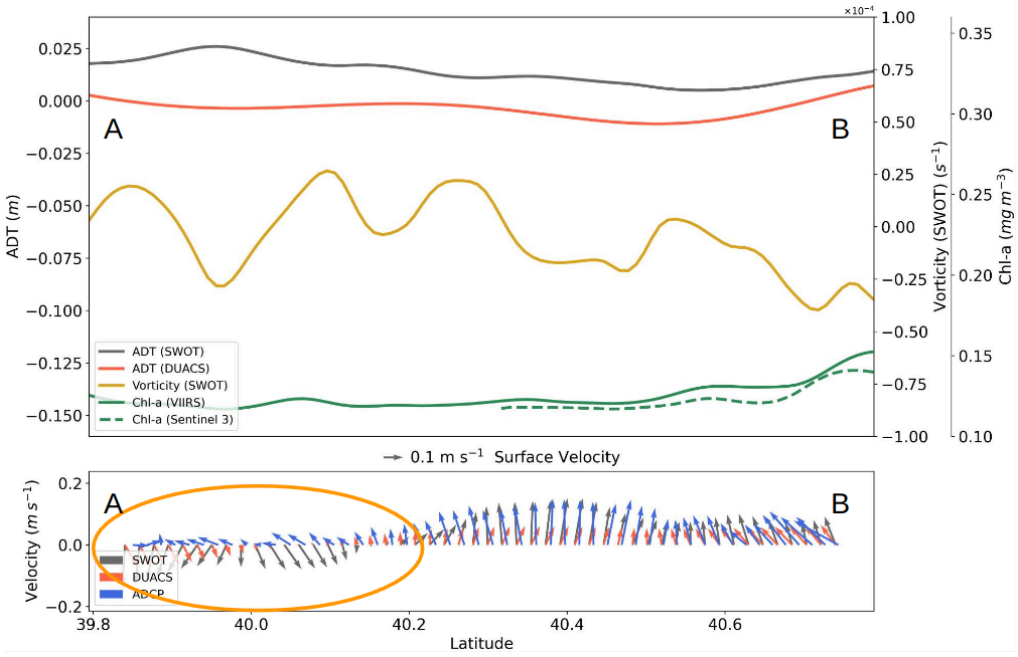

Fig.15: Values extracted from transect “A-B” shown in Fig. 14. The upper panel shows SWOT ADT (black), DUACS ADT (red), vorticity (yellow), VIIRS chlorophyll-a (solid green) and Sentinel-3 (dashed green). In the lower panel, geostrophic velocities from SWOT (black), DUACS (red) and ship ADCP (blue) are observed. A discrepancy between the ADCP and altimeter values is observed between 39.8 and 40.2°N (orange circle).

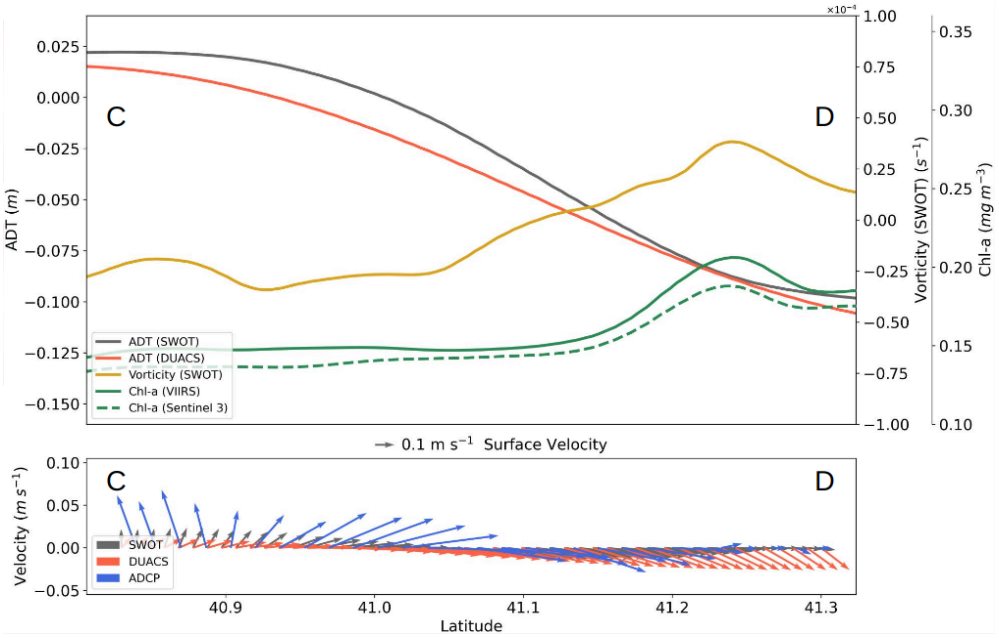

Fig.16: Values extracted from transect “C-D” shown in Fig. 14. The upper panel shows SWOT ADT (black), DUACS ADT (red), vorticity (yellow), VIIRS chlorophyll-a (solid green) and Sentinel-3 (dashed green). In the lower panel, geostrophic velocities from SWOT (black), DUACS (red) and ship ADCP (blue) are observed. A jet detected by SWOT and the vessel's ADCP is observed in the vicinity of the Balearic front.

Conclusions

During the 2-month stay (January 24, 2025 to March 24, 2025) at the MIO institute funded by the POGO-SCOR 2024 fellowship, different datasets were analyzed and combined. Although only two particular dates are emphasized in this report (May 4 and May 17), all available images for dates corresponding to the BioSWOT-Med cruise (April 21 to May 15) were analyzed and are available.

A submesoscale eddy detection algorithm, developed by Beckel et al. 2023, was adapted and applied during the BioSWOT-Med cruise period. After several tests, it was concluded that the algorithm failed to detect eddies correctly during the cruise period. This may have been due to the difficulty of using SST images in the region, as well as to the spiral nature of the eddies to be detected. The latter is considered given that a few days after the end of the cruise the eddy was detected correctly.

To better characterize the eddy dynamics and structure, chlorophyll-a data from VIIRS and Sentinel-3 were analyzed in conjunction with SWOT imagery, complementing the output of the detection algorithm. Likewise, it is worth highlighting the consistency in the ADT, geostrophic velocity and vorticity from SWOT against the observed submesoscale eddies. In particular, there was a strong correspondence between the velocity field provided by SWOT and a filament observed in the VIIRS and Sentinel-3 images on May 4th. However, the ADT local maxima and minima were found to be approximately 10 km away from the observed chlorophyll-a maxima.

The SWOT and DUACS altimetry products were compared. It was observed that the SWOT product allows better description of submesoscale structures and filaments due to its higher spatial resolution. In particular, a jet was detected which, could not be detected by the DUACS product, due to its spatial resolution,

Finally, the geostrophic velocities provided by SWOT and DUACS were compared with those measured by the vessel's ADCP during the cruise. It was observed that when crossing the Balearic front, the SWOT velocities corresponded very well with those measured by the ADCP, while the DUACS velocities failed to identify these features. We also observed regions where the velocities of both altimetry products did not match either in magnitude nor in direction with those measured by the ADCP. Then, there were others where they matched in direction but underestimated or overestimated magnitudes. This is why the velocity products provided by the altimeters, or merge of them, are not yet completely reliable to describe submesoscale features. Further progress should be made in this field since they are an excellent tool for the study of ocean dynamics at submesoscale magnitudes.

Acknowledgments

I would like to sincerely thank Dr. Andrea Doglioli for accepting to be my supervisor during my stay at the Mediterranean Institute of Oceanography (MIO), and for his continuous guidance and support. I am also deeply grateful to the entire MIO team for welcoming me and providing a stimulating and collaborative work environment. Finally, I extend my heartfelt thanks to the POGO-SCOR Fellowship Programme for funding this training through the POGO-SCOR 2024 Fellowship, which made this invaluable experience possible.

References

Becker, F., Romero, S. I., & Pisoni, J. P. (2023). Detection and characterization of submesoscale eddies from optical images: a case study in the Argentine continental shelf. International Journal of Remote Sensing, 44(10), 3146-3159.

Capet, X., Campos, E. J., & Paiva, A. M. (2008). Submesoscale activity over the Argentinian shelf. Geophysical Research Letters, 35(15).

Cao, H., Fox-Kemper, B., & Jing, Z. (2021). Submesoscale eddies in the upper ocean of the Kuroshio Extension from high-resolution simulation: Energy budget. Journal of Physical Oceanography, 51(7), 2181-2201.

Chen, X., Dewar, W., Chassignet, E., Bourassa, M., Morey, S., & Gopalakrishnan, G. (2022). On the feedback between air‐sea turbulent momentum flux and oceanic submesoscale processes. Journal of Geophysical Research: Oceans, 127(10), e2022JC018767.

Conejero, C., Renault, L., Desbiolles, F., McWilliams, J. C., & Giordani, H. (2024). Near-surface atmospheric response to meso-and submesoscale current and thermal feedbacks. Journal of Physical Oceanography, 54(3), 823-848.

Doglioli, A., Grégori, G., D'Ovidio, F., Bosse, A., Pulido, E., Carlotti, F., ... & Waggonet, E. M. (2024). BioSWOT Med. Biological applications of the satellite Surface Water and Ocean Topography in the Mediterranean.

Gula, J., Molemaker, M. J., & McWilliams, J. C. (2016). Topographic generation of submesoscale centrifugal instability and energy dissipation. Nature communications, 7(1), 12811.

Mahadevan, A. (2016). The impact of submesoscale physics on primary productivity of plankton. Annual review of marine science, 8(1), 161-184.

McWilliams, J. C. (2016). Submesoscale currents in the ocean. Proceedings of the Royal Society A: Mathematical, Physical and Engineering Sciences, 472(2189), 20160117.

Millot, C. (1987). Circulation in the western Mediterranean-sea. Oceanologica Acta, 10(2), 143-149.

Millot, C. (1999). Circulation in the western Mediterranean Sea. Journal of Marine Systems, 20(1-4), 423-442.

Millot, C., & Taupier-Letage, I. (2005). Circulation in the Mediterranean sea. The Mediterranean Sea, 29-66.
Le Vourche, J. (1992). Atlas of thermal fronts of the Mediterranean Sea derived from satellite imagery. Mem. l'Istitute oceanogrphique, Monaco, 16, 152.
Palomera, I., Olivar, M. P., Salat, J., Sabatés, A., Coll, M., García, A., & Morales-Nin, B. (2007). Small pelagic fish in the NW Mediterranean Sea: an ecological review. Progress in Oceanography, 74(2-3), 377-396.
Siegelman, L. (2020). Energetic submesoscale dynamics in the ocean interior. Journal of Physical Oceanography, 50(3), 727-749.
Strobach, E., Klein, P., Molod, A., Fahad, A. A., Trayanov, A., Menemenlis, D., & Torres, H. (2022). Local air‐sea interactions at ocean mesoscale and submesoscale in a western boundary current. Geophysical Research Letters, 49(7), e2021GL097003.
Su, Z., Wang, J., Klein, P., Thompson, A. F., & Menemenlis, D. (2018). Ocean submesoscales as a key component of the global heat budget. Nature communications, 9(1), 775.
Thomas, L. N., Tandon, A., & Mahadevan, A. (2008). Submesoscale processes and dynamics. Ocean modeling in an Eddying Regime, 177, 17-38.
Zatsepin, A., Kubryakov, A., Aleskerova, A., Elkin, D., & Kukleva, O. (2019). Physical mechanisms of submesoscale eddies generation: evidences from laboratory modeling and satellite data in the Black Sea. Ocean dynamics, 69, 253-266.
Zhang, Z., Miao, M., Qiu, B., Tian, J., Jing, Z., Chen, G., ... & Zhao, W. (2024). Submesoscale eddies detected by SWOT and moored observations in the Northwestern Pacific. Geophysical Research Letters, 51(15), e2024GL110000.